Article

Analysis of a Double Aging Process in a Maraging 300 Steel Fabricated by Selective Laser Melting, Using the Design of Experiments Technique

Inés Pérez-Gonzalo [1], Alejandro González-Pociño [1], Florentino Alvarez-Antolin [1,*] and Laura del Rio-Fernández [2]

1   Materials Science and Metallurgic Engineering Department, University of Oviedo, Independencia 13, 33004 Oviedo, Spain; uo225790@uniovi.es (I.P.-G.); gonzalezpalejandro@uniovi.es (A.G.-P.)
2   ArcelorMittal Global R&D Asturias, P.O. Box 90, 33400 Avilés, Spain; laura.delriofernandez@arcelormittal.com
*   Correspondence: alvarezflorentino@uniovi.es

Abstract: This study aims to optimize the aging treatment of a maraging 300 steel, without prior austenitizing, manufactured by the selective laser melting (SLM) technique. The study includes the analysis of a double aging process. In addition, the impact of the aging treatment on corrosion resistance in 3.5 wt.% NaCl solution was analyzed. The research technique followed was a factorial design of experiments with three factors and two levels, performing one replicate of each experiment. The results show that excellent mechanical properties can be achieved by omitting the solubilization treatment prior to aging. The highest hardness and tensile strength were achieved by performing a double aging at 460 °C for 8 h. Under these conditions, the maximum hardness exceeded 615 HV and the tensile strength was over 2140 MPa. Aging at 520 °C caused the formation of reverse austenite. The aging temperature was the only factor that had a significant effect on the formation of reverse austenite. It should be noted that the holding time at this temperature did not have a significant effect. The corrosion resistance, in 3.5 wt.% NaCl aqueous solution, increased in the aged samples compared to the as-printed sample. Samples overaged at 520 °C showed the best corrosion resistance. It can be concluded that the predominant cathodic reaction taking place is the reduction of oxygen dissolved in the electrolyte.

Keywords: maraging steel; aging; selective laser melting; linear polarization resistance; reverse austenite

1. Introduction

Maraging steels exhibit excellent properties due to the possibility of martensitic transformation offered by the Fe-Ni binary system when the weight percentage exceeds 8%, and the potential for aging of this martensite when the alloy contains elements such as Ti, Al, Mo, or Co [1–3]. These steels are widely used in applications requiring high strength and good toughness, i.e., in aircraft parts or nuclear reactor components [4].

The main hardening promoting precipitates are $Ni_3(Ti, Mo)$ and Fe_2Mo-Laves [5–8]. $Ni_3(Ti, Mo)$-type precipitates tend to form in the early stages of aging. Other possible precipitates that promote the hardening of these alloys are $\beta(NiAl)$, $\sigma(FeMo; FeTi)$, $\mu(Fe_7Mo_6)$, and $\chi(Fe_{36}Cr_{12}Mo_{10})$ [6,9–11]. Structurally hardening precipitates exhibit a matrix-coherent interface that increases yield strength and ultimate stress as a result of the interaction of this interface with dislocations [1]. Ti is the most effective strengthening agent in these steels.

The C content should be avoided in order to prevent the formation of Ti carbides [12]. Excessively high austenitizing temperatures may favor an increase in austenitic grain size [13,14], weakening the hardening of the aged martensite [15]. Nonetheless, low temperatures may be insufficient to obtain a fully austenitic structure since they may foster the permanence of Laves phases, with AB_2 stoichiometry of the $(Ti, Mo) (Fe, Cr, Ni)_2$ type, which remain integrated and sparsely distributed in the martensite laths after cooling [14].

They exhibit a compact hexagonal closed-packed crystal structure (HCP), and their size can vary around 200 nm [16,17]. These phases can be formed at temperatures around 550 °C and do not dissolve entirely until above 900 °C [14]. Austenitizing temperatures below 900 °C may not lead to the dissolution of the Laves phases. Low austenitizing temperatures cause the Laves precipitates to reach large sizes. Yet, this reduces the volume fraction of very fine Laves precipitates that could form during aging. Selection of the austenitizing temperature enables the ratio of Laves precipitates to be changed between small, formed during aging, and large, formed during austenitizing [17]. The presence of retained austenite and Laves phases is detrimental to the mechanical strength [14]. These precipitates have a negative effect on toughness [17].

The austenite formed during aging is called reverse austenite. The percentage of this austenite increases with higher temperatures and longer aging times [18]. The formation of reverse or inverse austenite is a consequence of the enrichment of the austenite in stabilizing elements [19]. Li and Yin suggest that reverse austenite results from the partial dissolution of $Ni_3(Ti, Mo)$ and the formation of Fe_2Mo [20]. This Ni-enriched austenite is particularly stable and does not transform when cooled to room temperature after aging [21–24].

Traditional martensitic steels with 18% Ni (maraging 300) mainly use Ni_3Ti, combined with Laves precipitates to achieve the hardening effect [7]. These steels are particularly expensive mainly due to the presence of alloying elements, such as Ni and Co [16]. The chemical composition range of the main alloying elements of a maraging 300 steel are 18–19% Ni, 8.5–9.5% Co, 4.6–5.2% Mo, and 0.5–0.8% Ti, with a maximum C content of 0.03% [25].

The selective laser melting (SLM) manufacturing process is categorized within the powder bed fusion (PBD) processes of additive manufacturing (AM) [10]. The SLM process makes it possible to manufacture chemically homogeneous parts, without dentritic segregation, and with complex geometries [26–28]. ArcelorMittal Innovation, Research and Investment, S.L. has this technology available at its facilities in Spain. These additive manufacturing processes can fabricate tridimensional objects by means of digital inputs [3]. The manufacturing process consists of the repetitive addition of thin layers of metallic powder on a horizontal platform that moves vertically (Z-axis). Each layer is only a few microns thick. A laser scans the powdered surface, melting those particles that, when solidified, will become part of a layer of the final part. Once the layer has been scanned, the adjustable platform is lowered a few microns along the Z-axis, and a new layer of powder is deposited on the existing substrate. When all the layers that constitute the final component have melted and solidified, the remaining unmelted particles are removed [29]. This manufacturing technique involves complex physical phenomena, such as the heating, melting, and solidification of a metallic powder [8]. The main process parameters are laser power, layer thickness, scan speed, and scan spacing [30]. These parameters provide a characterization of the process in terms of energy density [31].

Ni steels of 18% show a virtually martensitic structure after fabrication by the SLM process. Given that the molten mass is very small and the cooling rate very high, no austenitizing treatment would be necessary to obtain a fully hardened state [27]. The standard practice for martensitic steels with 18% Ni is to carry out the aging treatment in a single step. However, several aging cycles can improve the tensile strength and toughness considerably, albeit with significant reductions in the ductility and impact strength [32]. The double aging treatment appears to increase the strength and fatigue strengths, especially in high-humidity conditions [33].

The correlation between the microstructure and the mechanical properties of additively manufactured M300 steel under different heat treatment processes has been widely studied. However, previous studies have rarely focused on corrosion behavior. While aging precipitation treatments improve the mechanical properties of additive-manufactured maraging steels, several authors have also reported that these treatments tend to worsen their corrosion resistance [34,35]. From a practical application standpoint, the poor corrosion resistance of M300 steels compared to other tool steels or stainless steels represents

a major challenge for SLM-processed martensitic aged steel parts [36]. As in the mechanical behavior of the material, corrosion resistance in martensitic steels is influenced by both the formation of precipitates and the presence of reversed austenite [37–39]. High nickel (Ni) and molybdenum (Mo) contents and a lack of carbides provide better corrosion resistance [39]. The same applies to the presence of reversed austenite in martensitic steels [23,40,41]. However, there are still open questions concerning the relationships between the specimen microstructure, the corrosion mechanism, and the effect of aging treatments on its corrosion behavior.

The aim of this study was to optimize the aging treatment of a maraging 300 steel fabricated by the SLM process, including the study of a double aging process and considering that the maximum values of hardness and ultimate strength of this alloy fabricated by conventional casting are 550–590 HV and 1800–2000 MPa, respectively [42,43]. The effect of the aging treatment on the corrosion resistance in a slightly acidic solution (pH $\approx$ 5) 3.5 wt.% NaCl aqueous solution was also analyzed.

2. Materials and Methods

Table 1 shows the chemical composition of the metallic powder used (Carpenter Technology Corporation, Philadelphia, PA, USA). Figure 1 shows a predominantly spherical geometry with an average size of 32.26 μm. The metallic powder was obtained through a previous process of atomization. The 10th percentile was 20.01 μm, and the 90th percentile was 50.99 μm. Printing was carried out on the RenAM500Q (RENISHAW, Wotton-under Edge, England) selective laser melting machine owned by Arcelormittal Innovation, Research and Investment, S.L. The laser power used was 250 W, the scan spacing was 80 μm, and the scan speed was 1000 mm/s. The layer thickness was 50 μm. The laser scanning sequence was as follows: orthogonal scanning, cross scanning, and S-scanning. The printer used includes a 200 W fiber laser (Yb: YAG, wavelength: 1075 nm, SPI). The fabricated samples had a relative density higher than 99.8%, with a confidence interval of 95%.

Table 1. Chemical composition of the metallic powder used in the SLM process (wt.%).

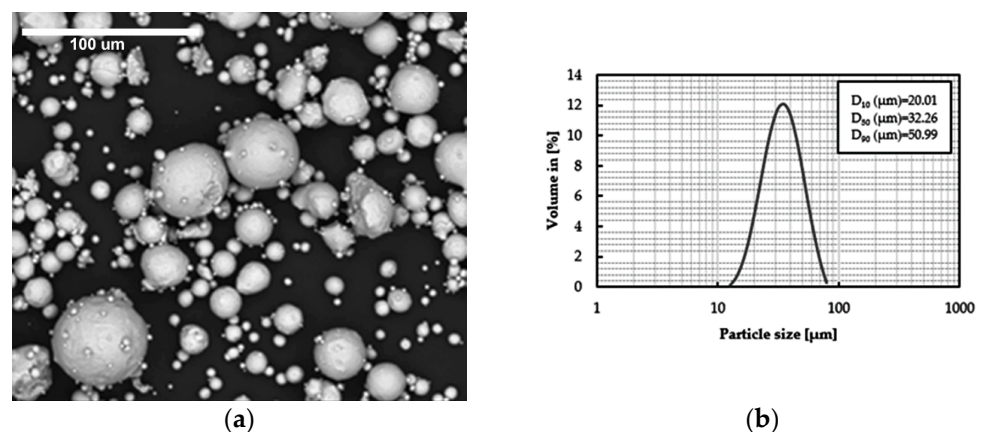| Ni	Co	Mo	Ti	Al	Fe
18.0	9.0	5.0	0.7	0.1	Balance

Figure 1. Metallic powder used in the SLM process. (**a**) Scanning electron microscope (SEM) image of a random sample; (**b**) particle size distribution.

The research methodology followed was a factorial design of experiments with 3 factors, 2 levels and 8 experiments [44]. The purpose of a design of experiments is to deliberately modify the normal working conditions in order to produce changes in some of the responses under study, for instance, the tensile strength of a material. These changes are made on certain factors, which have been previously selected. The design of experiments

is called full factorial when the number of experiments coincides with 2^k, where k is the number of factors to be studied and 2 is the number of levels applied to each of those factors [45–47]. The response of a factor is the variable to be analyzed. Therefore, the responses to be analyzed could be the hardness of a material or its breaking strain. The effect of a factor is defined as the variation of the response function as a consequence of the variation of that factor. According to the above, main effects are those effects calculated from each factor separately, i.e., they could be defined as the change in the response function when varying a given factor from its lowest level to its highest level [48]. Conversely, 2-factor interactions are defined as the variation between the average effect of one factor with the other factor at its low level and the average effect of the same factor with the other factor at the high level. Interactions between several factors are defined analogously [44]. The influence of the main effects on the response function tends to be greater than the importance of the 2-factor interactions, and these in turn greater than the 3-factor interactions and so forth. A given effect could be defined as significant if it is too "uncommon" to be the result of chance. Design of experiments are used to try to locate factors with a significant effect. For this purpose, a significance test is performed for each effect, using the t-Student as the reference distribution.

To this end, a one-sided hypothesis test is used with a significance level of 5% ($\alpha = 0.05$), where the null hypothesis is to consider that the mean of each effect is 0 [47,48]. If, as a result of this analysis, there is sufficient evidence to reject this hypothesis, it can be considered as significant, with a confidence level of 95%. Table 2 shows the factors and levels analyzed and Table 3 shows the matrix of experiments. It is a factorial design of experiments where k = 3 and the total number of experiments is 8, using 2 replicates in each experiment [49].

Table 2. Factors and levels.

Factors			Levels	
Code	Factors Description	Units	Level −1	Level +1
A	Aging temperature	°C	460	520
B	Holding time	h	2	8
C	Number of treatments	--	1	2

Table 3. Matrix of experiments.

Experiment	A	B	C	Restricted Confusion Pattern
	Aging Temp. (°C)	Holding Time (h)	Number of Treatments	
1	460	2	1	
2	520	2	1	Factor A
3	460	8	1	Factor B
4	520	8	1	Factor C
5	460	2	2	Interaction AB
6	520	2	2	Interaction AC
7	460	8	2	Interaction BC
8	520	8	2	

Fry reagent (5 g $CuCl_2$ (Sigma-Aldrich, Co., Madrid, Spain), 40 mL HCl (Sigma-Aldrich, Co., Madrid, Spain), 25 mL ethanol (Sigma-Aldrich, Co., Madrid, Spain) and 30 mL DI water) was used as the etching solution to reveal the microstructure of the material after mechanical grinding and polishing. Optical microscopy and scanning electron microscopy were used to examine the microstructure. The optical microscope used was the NIKON Epiphot 200 model (Nikon, Tokyo, Japan). The scanning electron microscope (SEM) used was the JEOL JSM-5600 model, equipped with the characteristic X-ray scattering microanalysis system (JEOL, Nieuw-Vennep, The Netherlands). The percentage and types of precipitated crystalline phases were determined by means of X-ray diffraction with a Cu

X-ray tube. The diffractometer used was the PANalytical X'Pert Pro MPD (PANalytical B.V., Almelo, The Netherlands) of the Scientific and Technical Services of the University of Oviedo. The determination of the percentage of crystalline phases was established using the Rietveld structural refinement method. Vickers hardness was measured using a load of 294 N. The hardness value estimated in each experiment was the average value obtained from 15 hardness indentations. The tensile test was performed according to ASTM E08, using standardized INSTROM equipment (Instron, Norwood, MA, USA) with a displacement speed of 5 mm/min and a load limit of 100 kN. The tensile specimens had a reduced section length of 34 mm and a square section of side 6 mm.

Corrosion resistance was analyzed on a slightly acidic 3.5 wt.% NaCl (Merck kGaA, Darmstadt, Germany) aqueous solution on aged samples versus as-printed samples. A sample over-aged for 96 h at 520 °C was included in the analysis. The methodology followed was that of linear polarization resistance, according to the ASTM G59 standard [50].

Prior to each electrochemical experiment, the samples were mechanically grinded with 60, 240, 400, 600 and 1200 SiC sandpaper, washed with distilled water, degreased in acetone and ethanol, and then air dried. The electrochemical measurements were carried out by using a Metrohm DropSens® μStat-i 400s potentiostat/galvanostat controlled by the DropView 8400 software, for electrochemical data acquisition and analysis (Metrohm Dropsens SL., Oviedo, Spain). The electrochemical experiments were performed in a conventional three-electrode Teflon cell with 1 cm^2 test area, containing holes to fix the electrodes. The reference and auxiliary electrodes were the Ag(s)/AgCl(s) (3M KCl) and a 150 mm platinum wire, respectively, (both from Metrohm Dropsens SL., Oviedo, Spain) while the solution-treated, the aged and the as-printed samples were the working electrodes. The corrosion behavior of the samples was evaluated by the linear polarization resistance (LPR) technique. The corrosion tests were carried out in triplicate at room temperature (about 25 °C) in a potential range from -100 to $+100$ mV around the OCP with a scan rate of 1 mVs^{-1}. Before the potentiodynamic test, 7200s open-circuit potential (OCP) was applied for stabilization. Polarization resistance (Rp) and corrosion voltage (Ecorr) were automatically obtained from the Dropview 8400 software after the test was carried out. Icorr was obtained applying the Stern-Geary equation on the numerical outputs from the software.

3. Results

Figure 2 shows the microstructure in the as-printed state. Figure 2a,b correspond to optical micrographs and Figure 2c,d) correspond to micrographs obtained by scanning electron microscopy (SEM). The microstructure is predominantly ferritic, with no detectable presence of austenite. Figure 2c shows a fine structure that has been formed as a consequence of the high cooling rate after melting [51]. It can be observed that, in certain areas, this microstructure consists of very fine columnar "grains", Figure 2d. The orientation of these columnar "grains" almost coincides with the printing direction. This structure arises because of the preferential cooling direction, which coincides with the printing direction. The powder surrounding the component acts as an insulating layer, so that the main directions of heat loss are the result of two phenomena: conduction heat transfer through the substrate and convection heat transfer through the top layer [8]. These solidification structures are, in fact dendrites with very short lateral (secondary) arms [52,53].

Table 4 shows the hardness's achieved by performing 2 repetitions (block 1 and block 2). This table also shows the effects of the main factors and second-degree interactions. The effect of the repetitions is also shown. In the as-printed state, the hardness was 363.95 ± 13.18 HV (294 N), with a confidence level of 95%. The average value of the 8 experiments was 575.87 HV.
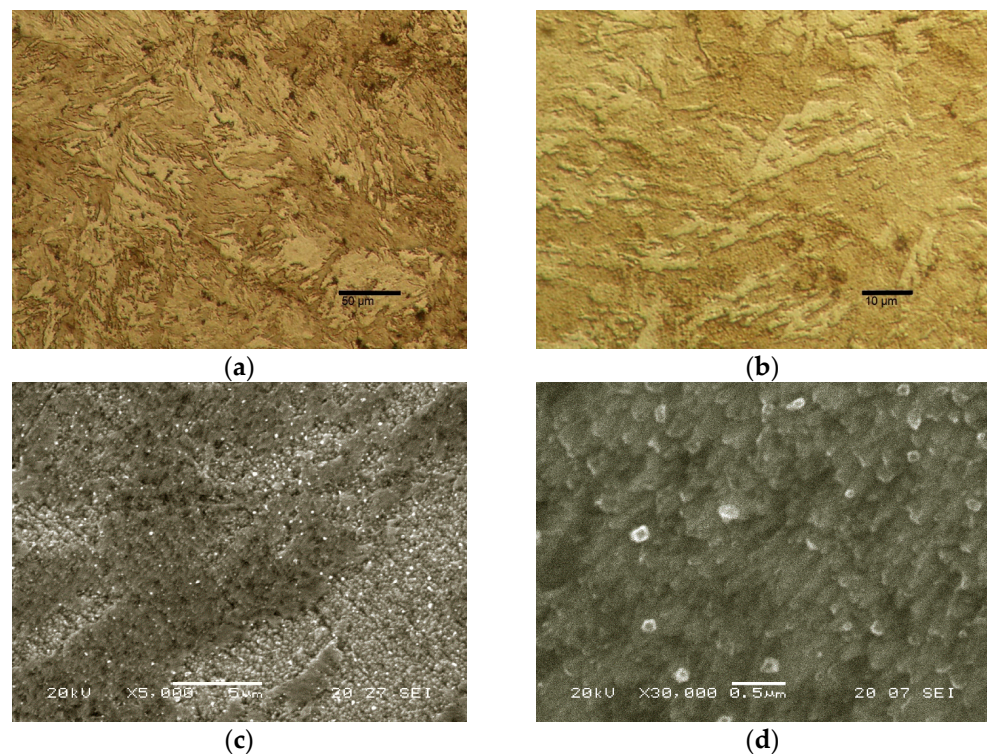
Figure 2. Microstructure in the as-printed state: (**a**) and (**b**) optical micrographs; (**c**) and (**d**) electron micrographs.

Table 4. Vickers hardness (294 N). Results from 2 repetitions and effects.

Experiment	Block 1	Block 2	Effect	Confounding Pattern
1	568	572	575.9	Average
2	564	566	−44.7	Factor A
3	604	604	−2.7	Factor B
4	550	546	8.2	Factor C
5	602	604	−26.2	Interaction AB
6	572	570	−14.2	Interaction AC
7	614	618	−11.2	Interaction BC
8	532	528	0.25	Block

Figure 3 shows the statistical analysis of the effects associated with hardness. Figure 3a shows the Pareto plot of the standardized effects using the t-Student as the reference distribution, with 8 degrees of freedom. The standard error was 1.118. An effect is considered significant if its standardized value exceeds the $t_{\alpha/2}$ value for a degree of freedom equal to 8. In this case, this value is 2.3. Factors A (aging temperature) and C (number of ages), together with the interactions AB, AC and BC, are found to have significant effects. It should be noted that the factor that has the most significant effect on hardness is the aging temperature and its interaction with the holding time. As a result, the greatest increase in hardness is obtained when the aging temperature is 460 °C and the holding time at this temperature is 8 h (interaction AB). In addition, in this same plot, an important effect of the interaction between the aging temperature and the number of aging treatments performed (interaction AC) is observed. Hardness increases when a double aging treatment is performed at 460 °C. Figure 3b shows the effect on hardness when varying between levels −1 and 1 of the main factors. It should be noted that the greatest increase in hardness is obtained by placing the aging temperature at level −1 (460 °C) compared to level 1 (520 °C). Similarly, Figure 3c shows the effect on hardness of the variation between levels −1 and 1 of the 2nd order interactions. All three have a significant effect; however, it is the AB

interaction that outstands the most, with the greatest increase in hardness being obtained when both are at their respective levels A= −1 (460 °C) and B = 1 (8 h). The results suggest that the peak hardness at 460 °C is reached later than at 520 °C. The hardness value after aging treatment at 460 °C for 8 h exceeded 600 HV. The hardness value reached at 520 °C for 8 h did not exceed 550 HV, while after aging treatment for 2 h it exceeded 560 HV. The holding times studied at 520 °C probably cause an over-aging of the precipitates and/or the beginning of the conversion process of martensite to austenite [54–56]. This would imply a decrease in hardness. It should also be noted that the increase in hardness that would result from placing factor A at level −1 (460 °C) would be reinforced by double aging (C = 1). As a continuation of this research, double aging processes will be studied at intermediate temperatures to those analysed and holding times shorter than 8 h. Figure 3d shows an estimation of the curves associated with the hardness of the material when factor C is placed at level 1 (double aging treatment). The increase in hardness due to a decrease in the aging temperature to 460 °C (Factor A = −1) must be highlighted. In turn, double aging treatment appears to increase the hardening potential.

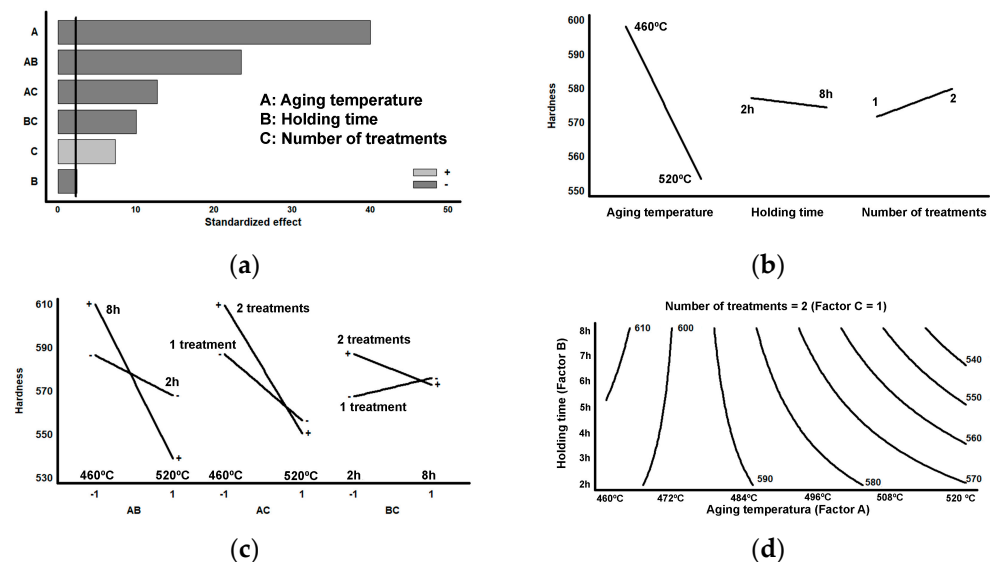**Figure 3.** Design of experiments plots associated with hardness: (**a**) Pareto chart; (**b**) main factors; (**c**) 2nd order interactions; (**d**) estimated level curve for two agings (C = 1).

Figure 4 shows two broken tensile specimens. Specimen (a) is aged, and specimen (b) is in the as-printed state. All aged specimens fractured without plastic deformation. However, the as-printed specimens showed plastic deformation before fracture.

Table 5 shows the results obtained on the true tensile strength, performing 2 repetitions (block 1 and block 2). This table includes the effects of the main factors and second-degree interactions together with the effect of the replications (block effect). In the as-printed condition, the true ultimate stress was 1050 MPa. This value is the average of 3 tests with a minimum value of 1048 MPa and a maximum value of 1052 MPa. The average value of the 8 experiments was 2015.8 MPa, which is almost a doubling of the ultimate strength with respect to the as-printed state.

Figure 5 shows the statistical analysis of the effects associated with the true ultimate stress. Figure 5a shows the Pareto plot of the standardized effects. The standard error is 11.619. Using the t-Student as the reference distribution, with 8 degrees of freedom, and a significance level of 0.05 ($\alpha = 0.05$), factors B (aging time) and the interactions AB, AC and BC were found to have significant effects. The selected parameters to maximize the tensile strength, according to Figure 5a, should be: aging temperature at 460 °C, long holding times (8 h) and double aging treatment. Figure 5b shows the effect on tensile strength of varying between levels −1 and 1 of the principal factors. Similarly, Figure 5c shows the

effect of the three 2nd order interactions. Although all three have a significant effect, it is the AB interaction that has the greatest effect. The greatest increase in strength would occur when factors A and B are at their respective levels −1 (460 °C) and +1 (8 h of aging), which would be compatible with the results achieved when analyzing hardness. On the other hand, if factor A is set to level −1 (460 °C) it should, in turn, set factor C to level +1 (double aging treatment). This result also coincides with that achieved in the hardness analysis. Setting factor B at its +1 level (aging treatment for 8 h), the interaction with factor C appears to be not very significant. From the joint analysis of the effect of the factors on hardness and tensile strength, it is observed that the aging temperature at 460 °C is more significant on hardness than on tensile strength, whereas the aging time seems to be more significant on tensile strength than on hardness. Figure 5d shows an estimation of the contour lines associated with the tensile strength when factor A is at its −1 level (460 °C). The increase in tensile strength with increasing aging time can be observed. It can be concluded that the highest hardness and strength would be achieved by performing a double aging treatment at a temperature of 460 °C for 8 h. It is important to consider that other authors who performed solubilization treatments prior to aging treatments achieved tensile strength values around 2000 MPa [27]. Therefore, no solubilization treatment would be necessary. for this SLM manufactured alloy to achieve good mechanical properties.

Figure 4. Broken tensile specimens: (**a**) aged specimen; (**b**) specimen in as-printed state.

Table 6 shows the results obtained on the maximum uniform deformation, performing 2 repetitions (block 1 and block 2). In the as-printed state, the maximum true strain was 4%. This value was the same in the 3 tensile tests performed. The average value resulting from the 8 experiments was a maximum true strain of 6.2%, an increase of approximately 55% over the non-aged specimens.

Table 5. True tensile strength (MPa). Results of 2 repetitions and effects.

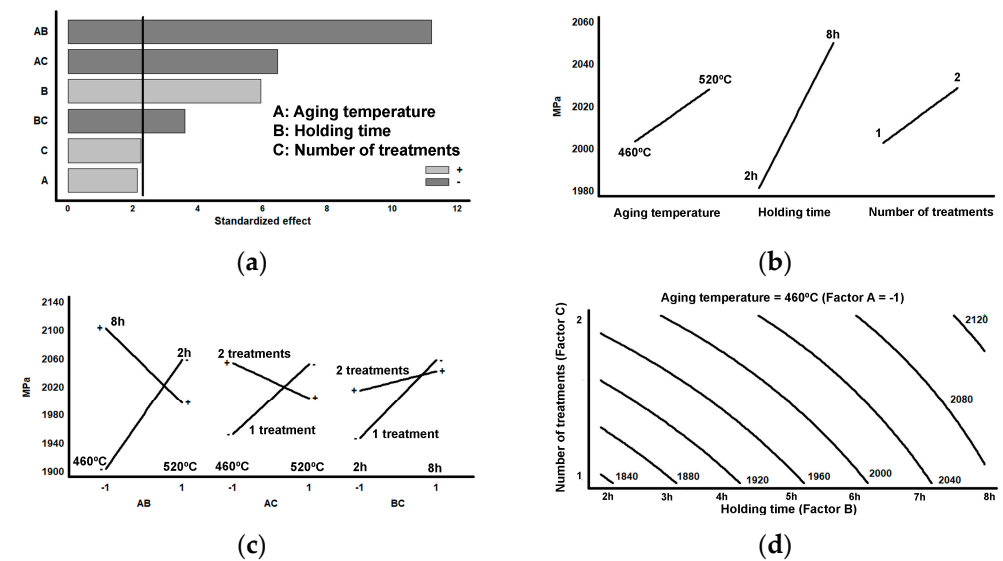| Experiment	Block 1	Block 2	Effect	Confounding Pattern
1	1842	1840	2015.8	Average
2	2059	2048	24.8	Factor A
3	2058	2071	69.1	Factor B
4	2079	2025	26.1	Factor C
5	1962	1971	−130.1	Interaction AB
6	2040	2088	−75.1	Interaction AC
7	2142	2141	−41.8	Interaction BC
8	1956	1931	−2.8	Block

(a)

(b)

(c)

(d)

Figure 5. Design of experiments plots associated with true tensile strength: (**a**) Pareto chart; (**b**) main factors; (**c**) 2nd order interactions; (**d**) estimated level curve for an aging temperature of 460 °C (A = 1).

Table 6. Maximum true uniform deformation (%). Results of 2 repetitions and effects.

Experiment	Block 1	Block 2	Effect	Confounding Pattern
1	5.2	6.1	6.2	Average
2	6.0	6.3	−0.2	Factor A
3	6.5	6.8	0.3	Factor B
4	6.4	5.7	0.2	Factor C
5	6.0	6.5	−0.4	Interaction AB
6	5.7	6.6	−0.2	Interaction AC
7	6.8	6.9	−0.1	Interaction BC
8	6.1	6.0	0.3	Block

Figure 6 shows the statistical analysis of the effects associated with the maximum uniform deformation. Figure 6a shows the Pareto plot of the standardized effects. The standard error was 0.178. Using the t-Student as the reference distribution, with 8 degrees of freedom and a significance level of 0.05 ($\alpha = 0.05$), the AB interaction was found to have a significant effect. Figure 6b shows the effect on the maximum uniform deformation of varying between levels −1 and 1 of the principal factors. Similarly, Figure 6c shows the effect of the three 2nd order interactions. Only the AB interaction has a significant effect, resulting that in order to increase the maximum uniform deformation both factors must be placed at the respective levels −1 (460 °C) and 1 (8 h). Figure 6d shows an estimation of the contour lines associated with the maximum uniform strain when factor A is at its −1 level

(460 °C). It can be seen that the steepest growth slope occurs with increasing aging time from 2 h to 8 h (factor B).
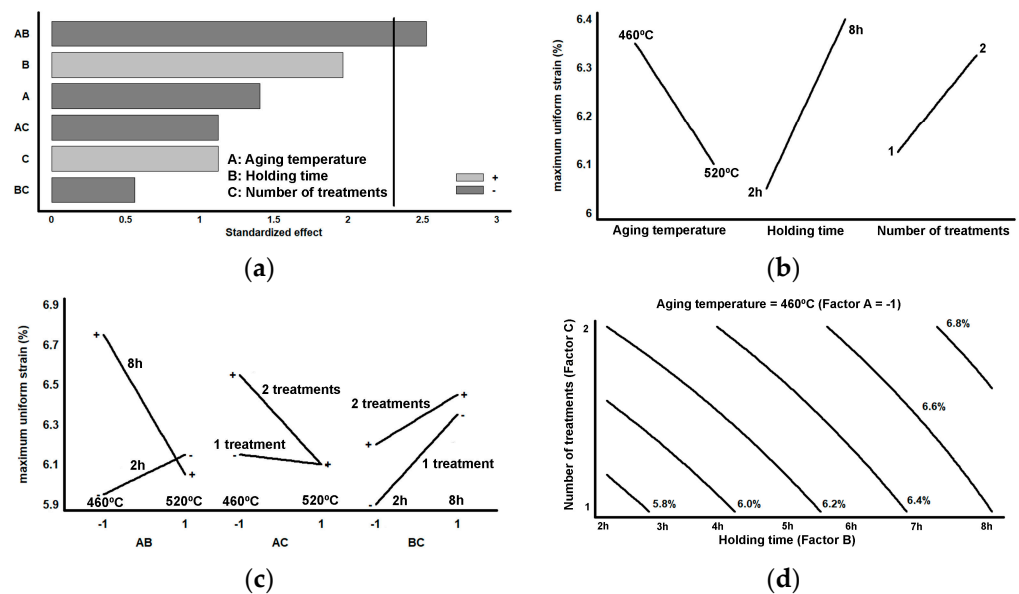

(a)

(b)

(c)

(d)

Figure 6. Design of experiments plots associated with the maximum true strain: (**a**) Pareto chart; (**b**) main factors; (**c**) 2nd order interactions; (**d**) estimated level curve for an aging temperature of 460 °C (A = −1).

Additionally, Table 7 shows the weight percentages of detected austenite by X-ray diffraction.

Table 7. Weight percentage of austenite.

Experiment	Rietveld Fitting	wt.%
"As print"	Rwp = 12.5 Chi^2 = 3.49	0
1	Rwp = 12.4 Chi^2 = 2.78	0
2	Rwp = 15.9 Chi^2 = 1.91	1
3	Rwp = 13.1 Chi^2 = 2.25	0
4	Rwp = 12.5 Chi^2 = 2.27	5
5	Rwp = 15.3 Chi^2 = 2.13	2
6	Rwp = 14.6 Chi^2 = 2.07	4
7	Rwp = 12.7 Chi^2 = 2.39	1
8	Rwp = 14.1 Chi^2 = 2.09	8

Figure 7 illustrates the statistical analysis of the effects related to the weight percentage of austenite. Figure 7a shows the Pareto diagram of the standardized effects. The resulting standard error is 0.25. Using the t-Student as the reference distribution, with 1 degree of freedom and a significance level of 0.05 (α = 0.05), an effect is defined as significant if its standardized value exceeds the value $t_{\alpha/2}$ = 12.7. Factor A (aging temperature) has a significant effect. Thus, since there was no austenite in the as-printed state, the formation of inverse austenite is associated with the aging temperature at 520 °C. This

result confirms that the aging temperature is the only factor that has a significant effect on the formation of inverse austenite. Other factors such as the holding time at this temperature or double aging treatment are not significant. Figure 7b shows the effect of the main factors. Similarly, Figure 7c depicts the effect of the three 2nd order interactions. Figure 7d shows an estimation of the contour lines associated with the amount of austenite when Factor A is at level 1 (520 °C). It can be observed that if the material is subjected to an aging temperature of 520 °C, there is a constant increase in the inverse austenite as the holding time (Factor B) increases. However, the latter factor is not of "significant" importance. These results confirm that the formation of reverse austenite is more sensitive to the aging temperature than to the aging time.
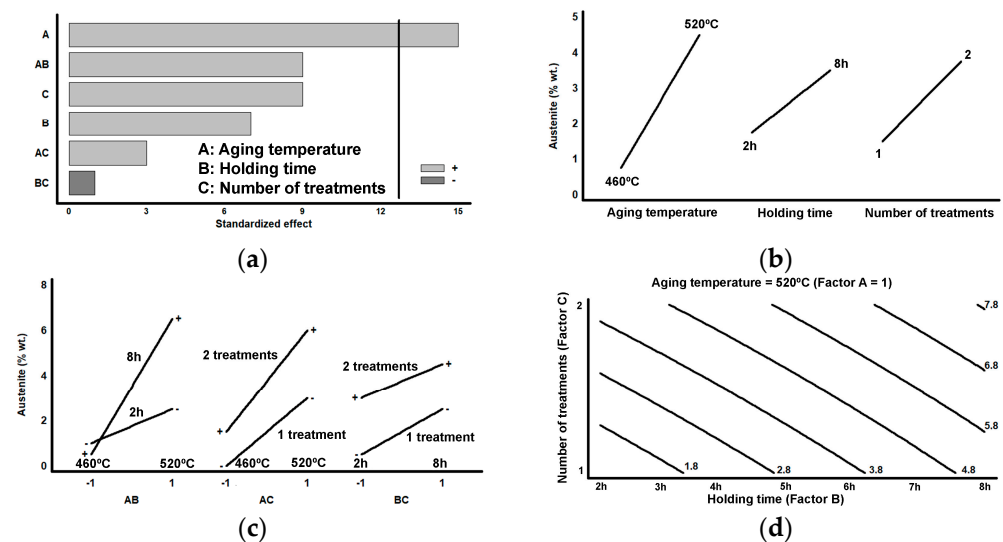

Figure 7. Design of experiments plots associated with the presence of austenite (wt.%): (**a**) Pareto chart; (**b**) main factors; (**c**) 2nd order interactions; (**d**) estimated contour line for an ageing temperature of 520 °C (A = 1).

Parallel to the design of experiments, an over-ageing treatment was carried out at 520 °C for 96 h. Figure 8 shows the microstructure obtained. The microstructure shows a rupture of the fine cellular structure that the material presented in the as-printed state, forming regular martensite blocks of fairly coarse size [51]. The breaking of cell boundaries and formation of regular martensite blocks is likely to be due to an increased reversion of martensite to austenite with longer aging times. However, the formation of reverse austenite is more sensitive to the aging temperature than to the holding time at the aging temperature [52]. Figure 8a shows the presence of reverse austenite after over-aging. Figure 8b shows a high density of Ni-rich structural hardening intermetallic compounds, which become visible due to the over-ageing to which the material was underwent [10,52,57].

Table 8 shows the comparative results of the corrosion test, using the linear polarization resistance method (LPR). The performance of the as-printed and aged simples was compared, including the sample over-aged 96 h at 520 °C. Experiment 7 corresponds to the highest hardness (double aging treatment for 8 h at 460 °C) and experiment 8 to the lowest hardness (double aging treatment for 8 h at 520 °C). Figure 9 shows the polarization curves. Heat treatment reduced the corrosion potential (Ecorr).

Maraging steel is prone to galvanic corrosion mainly due to the presence of intermetallic precipitates, such as $Ni_3(Ti, Al, Mo)$ on the ferritic matrix, the latter acting as an anode and these precipitates as cathodes [58]. However, this type of corrosion is not observed. The corrosion rate is slightly lower in the aged samples, which could be due to the formation of extremely fine precipitates [58]. It is observed that the as-printed sample has a higher corrosion potential than the aged samples. The aged samples, including the over-aged sample, show lower corrosion potential and lower corrosion current density than the as-

printed sample. In particular, the higher polarization resistance and lower corrosion density was found on the over-aged sample. The corrosion potential is a consequence of several simultaneous corrosion processes under non-equilibrium conditions, resulting in this case predominantly the reduction of the oxygen dissolved in the electrolyte, which favours the dissolution of Fe atoms when the martensite is more saturated in alloying elements. These results encourage a further study to deepen in those conditions that favour some cathodic reactions over others, the effect on the electric field of the double layer formed in the vicinity of the working electrode and the activation energy that acts as an energy barrier on the deselectronization process [59,60].
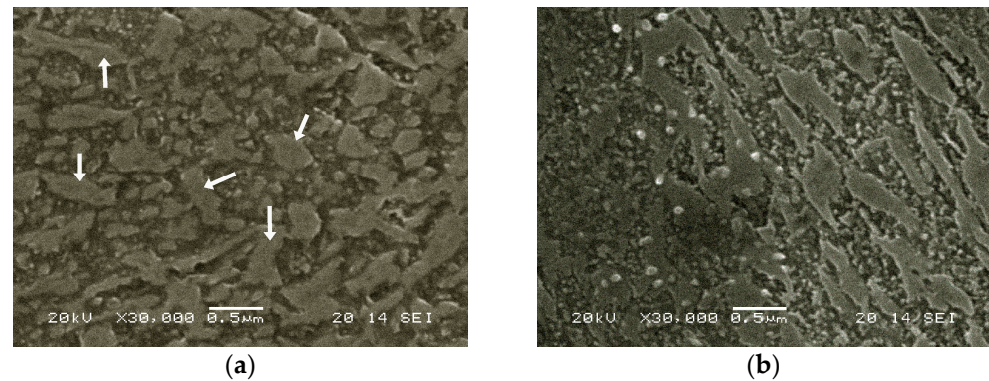

Figure 8. Microstructure of an over-aged specimen for 96 h at 520 °C: (**a**) the arrows show the presence of a high percentage of reverse austenite; (**b**) high density of Ni-rich intermetallic compounds.

Table 8. Linear polarization resistance (LPR) test results.

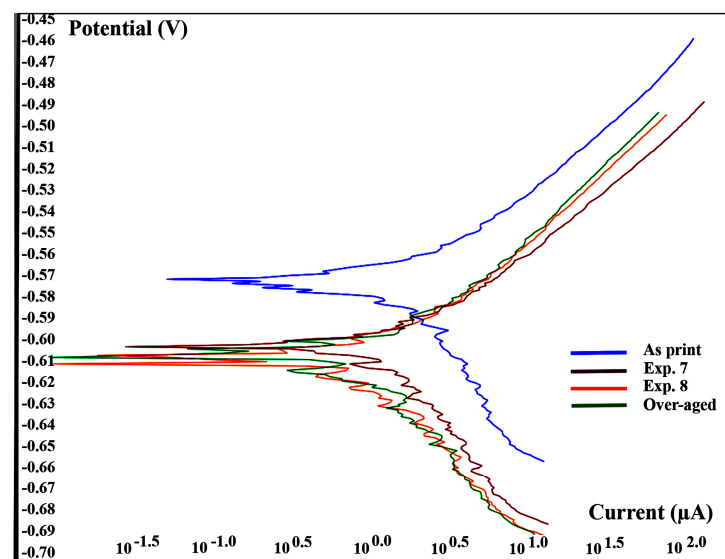| Sample	Rp (kΩ)	Ecorr (V vs. Ag/AgCl)	Icorr (µA/cm^2)
As-printed	8.24	−0.573	6.4
Experiment 7	9.33	−0.605	5.0
Experiment 8	13.75	−0.613	4.2
Over-aged (96 h at 520 °C)	15.53	−0.610	3.4

Figure 9. Polarization curves obtained by the linear polarization resistance method.

4. Conclusions

This study aims to optimize the aging treatment of a maraging 300 steel, which was fabricated using the SLM technique from spherical particles with an average size

of approximately 32 μm. The investigation was conducted without prior austenizing treatment and includes the analysis of a double aging process. Additionally, the impact of aging on corrosion resistance in a 3.5 wt.% NaCl solution was analyzed. The principal findings can be summarized as follows:

1. As a result of the statistical analysis of the design of experiments, it was found that the optimum treatment would be a double aging treatment at 460 °C for 8 h. Maximum hardness and tensile strength values were achieved under these conditions, being 618 HV and 2142 MPa, respectively.

2. These values are similar to those obtained by other authors who performed an austenizing treatment prior to aging, which confirms that excellent mechanical properties can be achieved by omitting this solubilization treatment prior to aging.

3. The presence of reverse austenite was found at the ageing temperature of 520 °C. The ageing temperature was the only factor that had a significant effect on the formation of reverse austenite. It should be noted that the holding time at this temperature did not have a significant effect.

4. Corrosion resistance, in aqueous solution of 3.5 wt.% NaCl, increased in the aged samples compared to the as-printed sample. No galvanic corrosion was observed during aging treatments, despite the theoretical anodic behaviour of ferrite against intermetallic precipitates derived from such aging treatment. The predominant electrochemical semireaction seems to be the reduction of the dissolved oxygen in the electrolyte, favouring the dissolution of Fe atoms when the martensite is more saturated in alloying elements. The heat treatment that appears to provide the best corrosion behaviour was over-aging treatment at 520 °C.

Author Contributions: Conceptualization, F.A.-A., A.G.-P. and L.d.R.-F.; methodology, F.A.-A. and A.G.-P.; validation, F.A.-A. and A.G.-P.; formal analysis, F.A.-A. and A.G.-P.; investigation, F.A.-A., A.G.-P., I.P.-G. and L.d.R.-F.; resources, L.d.R.-F.; data curation, F.A.-A., A.G.-P. and I.P.-G.; writing—original draft preparation, F.A.-A.; writing—review and editing, A.G.-P. and I.P.-G.; supervision, F.A.-A.; project administration, F.A.-A.; funding acquisition, L.d.R.-F. All authors have read and agreed to the published version of the manuscript.

Data Availability Statement: Data is contained within the article.

Conflicts of Interest: The authors declare no conflict of interest.

References

1. El-Fawkhry, M.K.; Eissa, M.; Fathy, A.; Mattar, T. Development of maraging steel with retained austenite in martensite matrix. *Mater. Today-Proc.* **2015**, *2*, 711–714. [CrossRef]

2. Jiang, S.; Wang, H.; Wu, Y.; Liu, X.; Chen, H.; Yao, M.; Gault, B.; Ponge, D.; Raabe, D.; Hirata, A.; et al. Ultrastrong steel via minimal lattice misfit and high-density nanoprecipitation. *Nature* **2017**, *544*, 460. [CrossRef]

3. Kolomy, S.; Sedlak, J.; Zouhar, J.; Slany, M.; Benc, M.; Dobrocky, D.; Barenyi, I.; Majerik, J. Influence of Aging Temperature on Mechanical Properties and Structure of M300 Maraging Steel Produced by Selective Laser Melting. *Materials* **2023**, *16*, 977. [CrossRef] [PubMed]

4. Rosenauer, A.; Brandl, D.; Ressel, G.; Lukas, S.; Monschein, S.; Stockinger, M.; Schnitzer, R. Influence of delta ferrite on the impact toughness of a PH 13-8 Mo maraging steel. *Mater. Sci. Eng. A-Struct. Mater. Prop. Microstruct. Process.* **2022**, *856*, 144024. [CrossRef]

5. Liu, P.; Stigenberg, A.H.; Nilsson, J.O. Quasi-crystalline and crystalline precipitation during isothermal tempering in a 12Cr-9Ni-4Mo maraging stainless-steel. *Acta Metall. Mater.* **1995**, *43*, 2881–2890. [CrossRef]

6. Huang, C.Y.; Yen, H.W. HRTEM investigations on nano precipitates in Custom 475 maraging stainless steel. *Mater. Charact.* **2021**, *178*, 111216. [CrossRef]

7. Wan, J.Q.; Ruan, H.H.; Ding, Z.Y.; Kong, L.B. A novel maraging stainless steel ultra-high-strengthened by multi-nanoprecipitations. *Scr. Mater.* **2023**, *226*, 115224. [CrossRef]

8. Habassi, F.; Houria, M.; Barka, N.; Jahazi, M. Influence of post-treatment on microstructure and mechanical properties of additively manufactured C300 maraging steel. *Mater. Charact.* **2023**, *202*, 112980. [CrossRef]

9. Escriba, D.M.; Materna-Morris, E.; Plaut, R.L.; Padilha, A.F. Chi-phase precipitation in a duplex stainless steel. *Mater. Charact.* **2009**, *60*, 1214–1219. [CrossRef]

10. Tan, C.L.; Zhou, K.S.; Ma, W.Y.; Zhang, P.P.; Liu, M.; Kuang, T.C. Microstructural evolution, nanoprecipitation behavior and mechanical properties of selective laser melted high-performance grade 300 maraging steel. *Mater. Des.* **2017**, *134*, 23–34. [CrossRef]

11. Halfa, H.; Seikh, A.H.; Soliman, M.S. Effect of Heat Treatment on Tensile Properties and Microstructure of Co-Free, Low Ni-10 Mo-1.2 Ti Maraging Steel. *Materials* **2022**, *15*, 2136. [CrossRef] [PubMed]

12. Chales, R.; Martins Cardoso, A.d.S.; Pires Garcia, P.S.; da Igreja, H.R.; de Almeida, B.B.; Noris, L.F.; Pardal, J.M.; Maior Tavares, S.S.; da Silva, M.M. Behavior of constitutive models from slow strain rate test of maraging 300 and 350 steels performed in several environmental conditions. *Int. J. Fract.* **2022**, *234*, 159–175. [CrossRef]

13. Rusanenko, V.V.; Edneral, A.F.; Libman, M.A. Structure and properties of titanium-free maraging alloys. *Phys. Met. Metallogr.* **2006**, *101*, 66–74. [CrossRef]

14. Lian, Y.; Ma, M.; Zhang, J.; Huang, J.; Gao, W.; Zhang, Z.; Zhao, C. Influence of Austenizing Temperature on the Microstructure and Mechanical Properties of an Fe-Cr-Ni-Mo-Ti Maraging Stainless Steel. *J. Mater. Eng. Perform.* **2019**, *28*, 5466–5475. [CrossRef]

15. Tavares, S.S.M.; Pardal, J.M.; Martins, T.R.D.; Schmitt, V.M.; Szlejf, J.F.V. Influence of Austenizing on the Mechanical Properties of Maraging 300 and Sae 4340 Steels—Comparative Study. *Mater. Res.-Ibero-Am. J. Mater.* **2017**, *20*, 39–46. [CrossRef]

16. Mahmoudi, A.; Ghavidel, M.R.Z.; Nedjad, S.H.; Heidarzadeh, A.; Ahmadabadi, M.N. Aging behavior and mechanical properties of maraging steels in the presence of submicrocrystalline Laves phase particles. *Mater. Charact.* **2011**, *62*, 976–981. [CrossRef]

17. Simm, T.H.; Sun, L.; Galvin, D.R.; Hill, P.; Rawson, M.; Birosca, S.; Gilbert, E.P.; Bhadeshia, H.; Perkins, K. The Effect of a Two-Stage Heat-Treatment on the Microstructural and Mechanical Properties of a Maraging Steel. *Materials* **2017**, *10*, 1346. [CrossRef]

18. Makhneva, T.M.; Sukhikh, A.A.; Dement'ev, V.B. Inverse Martensitic alpha -> gamma Transformation in Nanostructured Maraging Steels. *Met. Sci. Heat Treat.* **2017**, *59*, 473–478. [CrossRef]

19. Ancey-Rocchi, S.; Vidal, V.; Poulain, T.; Billot, T.; Bechet, D.; Binot, N.; Huleux, V.; Dehmas, M.; Delagnes, D. Influence of Austenitization Parameters on the Precipitation Sequence and the Chemical Homogenization of Austenite in a High-Performance Fe-Ni-Cr-Al-Ti-Mo Stainless Maraging Steel. *Metall. Mater. Trans. A-Phys. Metall. Mater. Sci.* **2021**, *52*, 4623–4635. [CrossRef]

20. Li, X.D.; Yin, Z.D. Reverted austenite during aging in 18ni(350) maraging-steel. *Mater. Lett.* **1995**, *24*, 239–242. [CrossRef]

21. Bai, Y.; Zhao, C.; Zhang, J.; Wang, H. Abnormal thermal expansion behaviour and phase transition of laser powder bed fusion maraging steel with different thermal histories during continuous heating. *Addit. Manuf.* **2022**, *53*, 102712. [CrossRef]

22. Zhang, C.; Wang, C.; Wang, A.; Zheng, C.; Liu, Z.; Liang, J.; Su, J.; Ge, Q. Effect of Aging on Transformation Behavior of Reverted Austenite and Toughness in Co-Free Maraging Stainless Steel. *J. Mater. Eng. Perform.* **2022**, *31*, 9850–9863. [CrossRef]

23. Khan, H.M.; Ozer, G.; Yilmaz, M.S.; Tarakci, G. Improvement of Corrosion Resistance of Maraging Steel Manufactured by Selective Laser Melting Through Intercritical Heat Treatment. *Corrosion* **2022**, *78*, 239–248. [CrossRef]

24. Conde, F.F.; Escobar, J.D.; Oliveira, J.P.; Jardini, A.L.; Bose Filho, W.W.; Avila, J.A. Austenite reversion kinetics and stability during tempering of an additively manufactured maraging 300 steel. *Addit. Manuf.* **2019**, *29*, 100804. [CrossRef]

25. Pepi, M.S. Effects of Prior Processing on the Service Life of an 18% Nickel Maraging Steel Helicopter Landing Mount. *J. Fail. Anal. Prev.* **2022**, *22*, 2423–2430. [CrossRef]

26. Angelastro, A.; Campanelli, S.L. An integrated analytical model for the forecasting of the molten pool dimensions in Selective Laser Melting. *Laser Phys.* **2022**, *32*, 026001. [CrossRef]

27. Kim, D.; Kim, T.; Ha, K.; Oak, J.-J.; Jeon, J.B.; Park, Y.; Lee, W. Effect of Heat Treatment Condition on Microstructural and Mechanical Anisotropies of Selective Laser Melted Maraging 18Ni-300 Steel. *Metals* **2020**, *10*, 410. [CrossRef]

28. Bae, K.; Kim, D.; Lee, W.; Park, Y. Wear Behavior of Conventionally and Directly Aged Maraging 18Ni-300 Steel Produced by Laser Powder Bed Fusion. *Materials* **2021**, *14*, 2588. [CrossRef]

29. Mumtaz, K.; Hopkinson, N. Top surface and side roughness of Inconel 625 parts processed using selective laser melting. *Rapid Prototyp. J.* **2009**, *15*, 96–103. [CrossRef]

30. Guo, Q.X.; Wang, Y.S.; Lin, J.H. Effect of additive and subtractive hybrid manufacturing process on the surface quality of 18Ni300 maraging steel. *Mater. Res. Express* **2023**, *10*, 056501. [CrossRef]

31. Morgan, R.; Sutcliffe, C.J.; O'Neill, W. Density analysis of direct metal laser re-melted 316L stainless steel cubic primitives. *J. Mater. Sci.* **2004**, *39*, 1195–1205. [CrossRef]

32. Tariq, F.; Naz, N.; Baloch, R.A. Effect of Cyclic Aging on Mechanical Properties and Microstructure of Maraging Steel 250. *J. Mater. Eng. Perform.* **2010**, *19*, 1005–1014. [CrossRef]

33. Rohit, B.; Muktinutalapati, N.R. Fatigue Behavior of 18% Ni Maraging Steels: A Review. *J. Mater. Eng. Perform.* **2021**, *30*, 2341–2354. [CrossRef]

34. Wang, L.; Dong, C.F.; Man, C.; Kong, D.C.; Xiao, K.; Li, X.G. Enhancing the corrosion resistance of selective laser melted 15-5PH martensite stainless steel via heat treatment. *Corros. Sci.* **2020**, *166*, 108427. [CrossRef]

35. Hong, Y.; Dong, D.; Zou, G.; Li, Y.; Lin, S.; Kuang, T.; Wu, Y.; Dai, M. The corrosion response of the heterogeneous nitriding structure originated from the laser additive manufactured steel. *Corros. Sci.* **2023**, *218*, 111188. [CrossRef]

36. Godec, M.; Podgornik, B.; Kocijan, A.; Donik, C.; Balantic, D.A.S. Use of plasma nitriding to improve the wear and corrosion resistance of 18Ni-300 maraging steel manufactured by selective laser melting. *Sci. Rep.* **2021**, *11*, 3277. [CrossRef]

37. Wang, L.; Dong, C.F.; Yu, Q.; Man, C.; Hu, Y.B.; Dai, Z.B.; Li, X.G. The Correlation Between the Distribution/Size of Carbides and Electrochemical Behavior of 17Cr-1Ni Ferritic-Martensitic Stainless Steel. *Metall. Mater. Trans. A-Phys. Metall. Mater. Sci.* **2019**, *50*, 388–400. [CrossRef]

38. Zhang, Z.Y.; Zhao, H.; Zhang, H.Z.; Yu, Z.S.; Hu, J.; He, L.; Li, J. Effect of isothermal aging on the pitting corrosion resistance of UNS S82441 duplex stainless steel based on electrochemical detection. *Corros. Sci.* **2015**, *93*, 120–125. [CrossRef]

39. Bae, K.; Shin, D.; Kim, J.H.; Lee, W.K.; Jo, I.; Lee, J.H. Influence of Post Heat Treatment Condition on Corrosion Behavior of 18Ni300 Maraging Steel Manufactured by Laser Powder Bed Fusion. *Micromachines* **2022**, *13*, 1977. [CrossRef]

40. Man, C.; Dong, C.F.; Kong, D.C.; Wang, L.; Li, X.G. Beneficial effect of reversed austenite on the intergranular corrosion resistance of martensitic stainless steel. *Corros. Sci.* **2019**, *151*, 108–121. [CrossRef]

41. Lei, X.W.; Feng, Y.R.; Zhang, J.X.; Fu, A.Q.; Yin, C.X.; Macdonald, D.D. Impact of Reversed Austenite on the Pitting Corrosion Behavior of Super 13Cr Martensitic Stainless Steel. *Electrochim. Acta* **2016**, *191*, 640–650. [CrossRef]

42. Lima, V.X.; Barros, I.F.; De Abreu, H.F.G. Influence of Solution Annealing on Microstructure and Mechanical Properties of Maraging 300 Steel. *Mater. Res.* **2017**, *20*, 10–14. [CrossRef]

43. Pardal, J.M.; Tavares, S.S.M.; Fonseca, M.P.C.; da Silva, M.R.; Neto, J.M.; Abreu, H.F.G. Influence of temperature and aging time on hardness and magnetic properties of the maraging steel grade 300. *J. Mater. Sci.* **2007**, *42*, 2276–2281. [CrossRef]

44. Kumar, S.; Bablu, M.; Janghela, S.; Misra, M.K.; Mishra, R.; Ranjan, A.; Prasad, N.E. Factorial design, processing, characterization and microstructure analysis of PIP-based C/SiC composites. *Bull. Mater. Sci.* **2018**, *41*, 17. [CrossRef]

45. Srinivasan, P.M.; Dharmakkan, N.; Vishnu, M.D.S.; Prasath, H.; Gogul, R. Thermal conductivity analysis of Al_2O_3/water-ethylene glycol nanofluid by using factorial design of experiments in a natural convection heat transfer apparatus. *Hem. Ind.* **2021**, *75*, 341–352. [CrossRef]

46. Nassif, N.; Zeiada, W.; Al-Khateeb, G.; Haridy, S.; Altoubat, S. Assessment of Punching Shear Strength of Fiber-reinforced Concrete Flat Slabs Using Factorial Design of Experiments. *Jordan J. Civ. Eng.* **2022**, *16*, 139–154.

47. Mouelhi, M.; Marzouk, I.; Hamrouni, B. Optimization studies for water defluoridation by adsorption: Application of a design of experiments. *Desalination Water Treat.* **2016**, *57*, 9889–9899. [CrossRef]

48. Maskovic, M.; Jancic-Stojanovic, B.; Malenovic, A.; Ivanovic, D.; Medenica, M. Assessment of Liquid Chromatographic Method Robustness by Use of Plackett-Burman Design. *Acta Chromatogr.* **2010**, *22*, 281–296. [CrossRef]

49. Nurulhuda, A.; Hafrzzal, Y.; Izzuddin, M.Z.M.; Sulawati, M.R.N.; Rafidah, A.; Suhaila, Y.; Fauziah, A.R. Analysis on Flexural Strength of A36 Mild Steel by Design of Experiment (DOE). In Proceedings of the International Research and Innovation Summit (IRIS), Melaka, Malaysia, 6–7 May 2017.

50. *ASTM G59-23*; Standard Test Method for Conducting Potentiodynamic Polarization Resistance Measurements. ASTM International: West Conshohocken, PA, USA, 2023. [CrossRef]

51. Yan, X.; Chen, C.; Chang, C.; Dong, D.; Zhao, R.; Jenkins, R.; Wang, J.; Ren, Z.; Liu, M.; Liao, H.; et al. Study of the microstructure and mechanical performance of C-X stainless steel processed by selective laser melting (SLM). *Mater. Sci. Eng. A-Struct. Mater. Prop. Microstruct. Process.* **2020**, *781*, 139227. [CrossRef]

52. Yin, S.; Chen, C.; Yan, X.; Feng, X.; Jenkins, R.; O'Reilly, P.; Liu, M.; Li, H.; Lupoi, R. The influence of aging temperature and aging time on the mechanical and tribological properties of selective laser melted maraging 18Ni-300 steel. *Addit. Manuf.* **2018**, *22*, 592–600. [CrossRef]

53. Jaegle, E.A.; Sheng, Z.; Kuernsteiner, P.; Ocylok, S.; Weisheit, A.; Raabe, D. Comparison of Maraging Steel Micro- and Nanostructure Produced Conventionally and by Laser Additive Manufacturing. *Materials* **2017**, *10*, 8. [CrossRef]

54. Shamantha, C.R.; Narayanan, R.; Iyer, K.J.L.; Radhakrishnan, V.M.; Seshadri, S.K.; Sundararajan, S.; Sundaresan, S. Microstructural changes during welding and subsequent heat treatment of 18Ni (250-grade) maraging steel. *Mater. Sci. Eng. A* **2000**, *287*, 43–51. [CrossRef]

55. Kempen, K.; Yasa, E.; Thijs, L.; Kruth, J.P.; Van Humbeeck, J. Microstructure and mechanical properties of selective laser melted 18Ni-300 steel. *Phys. Procedia* **2011**, *12*, 255–263. [CrossRef]

56. Gao, P.; Jing, G.; Lan, X.; Li, S.; Zhou, Y.; Wang, Y.; Yang, H.; Wei, K.; Wang, Z. Effect of heat treatment on microstructure and mechanical properties of Fe–Cr–Ni–Co–Mo maraging stainless steel produced by selective laser melting. *Mater. Sci. Eng. A* **2021**, *814*, 141149. [CrossRef]

57. Tewari, R.; Mazumder, S.; Batra, I.S.; Dey, G.K.; Banerjee, S. Precipitation in 18 wt% Ni maraging steel of grade 350. *Acta Mater.* **2000**, *48*, 1187–1200. [CrossRef]

58. Ahmadkhaniha, D.; Moller, H.; Zanella, C. Studying the Microstructural Effect of Selective Laser Melting and Electropolishing on the Performance of Maraging Steel. *J. Mater. Eng. Perform.* **2021**, *30*, 6588–6605. [CrossRef]

59. Jiang, Y.; Ai, Y.; Wang, Q. Study on Corrosion Resistance of 00Cr13Ni7Co5Mo4W Maraging Stainless Steel in Seawater. *Mech. Eng. Mater. Sci. Civ. Eng.* **2013**, *274*, 402–405. [CrossRef]

60. El-Mahdy, G.A.; Hegaz, M.M.Y.; Heakal, F.E.-T.; Mahmoud, H.E.; Fathy, A.M.; Sayed, F.M. Electrochemical Behavior of Maraging Steel in Chloride Containing Environment. *Int. J. Electrochem. Sci.* **2013**, *8*, 2816–2825. [CrossRef]